Journal of Applied Fluid Mechanics, Vol. 11, No. 3, pp. 585-595, 2018.
Available online at www.jafmonline.net, ISSN 1735-3572, EISSN 1735-3645.
DOI: 10.29252/jafm.11.03.28239

Numerical Investigation on Temperature and Flow Characteristics of a Tornado-Like Vortex by using Large-Eddy Simulation

K. Li[1, 3†], M. Xiang[2], Y. Hu[3], X. L. Huang[3] and H.Y. Qi[3]

[1] *School of Energy and Environment, Inner Mongolia University of Science and Technology, Baotou, Inner Mongolia, 014010, China*
[2] *Institute of Aerospace and Material Engineering, National University of Defense Technology, Changsha, Hunan, 410073, China*
[3] *Institute of Thermal Engineering, Tsinghua University, Beijing 100084, China*

†*Corresponding Author Email: kelitsinghua@hotmail.com*

(Received July 20, 2017; accepted November 6, 2017)

ABSTRACT

The present work is about numerical simulations of the tornado-like vortex flow generated by our group based on LES techniques which is executed on a three-dimensional computational grid and results have been compared with experimental ones. Different subgrid-scale stress model and finite volume method are adopted to solve the low Mach number compressible Navier-Stokes equations using the different computational domain and boundary conditions, which are mainly to assess the model feasibility. All the simulations were performed using ANSYS FLUENT14.5 in consistency with the real experimental model which avoided the performances of the different techniques and turbulence models introducing other variables. Numerical results suggest that the vacuum degree, temperature difference and the rotation strength decayed in the axial and radial direction regularly changed with inlet gauge pressure p0 from 100 to 400 kPa which are consistent with experimental results. The accurate numerical simulation of this specific flow, resulting in an improved prediction capability of the flow and thermal properties of tornado-like vortex, could allow a correct estimation of the vacuum and energy separating performance of this device in strong rotating jet operation. Furthermore, computational results illustrate that strong rotating jet turbulent flow under the conditions of the certain pressure, temperature, velocity profiles and distribution can formed tornados-like vortex evolution and maintaining mechanism due to a large gradient in radial temperature, pressure and velocity balanced by inertia force, centrifugal force and rotational kinetic energy dissipation.

Keywords: Large-eddy simulation; Tornado-like vortex jet; Ranque-Hilsch effect; Vacuum degree; Energy separation.

NOMENCLATURE

D	dissipation term	T	temperature
k	turbulent kinetic energy	U	total velocity magnitude
h	enthalpy	u	velocity
p	static pressure (absolute)	v_t	tangential velocity
p_0	inlet gauge pressure	w	axial velocity
p_{vc}	vacuum degree		
P	production term	θ	spiral angle
Pr	prandtl number	κ	von Kármán constant
Q_l	standard volume flow rate	μ	dynamic viscosity
q	subgrid-scale heat flux	ν	kinematic viscosity
R	universal gas constant	ρ	density
r	radius	ω	vorticity

1. INTRODUCTION

Tornado in nature is a strong three-dimensional swirling turbulent flow and cause severe damages compared to other wind induced disasters, which need numerous detailed information of flow structure to understand it. Jones (Jones, 2015) and Richard (Richard, 2013) review the researches on this field recently, indicating that many researchers (Tari, Gurka, and Hangan, 2010; Ishihara, Oh, and Tokuyama, 2011; Diwakar and Horia, 2012; Lisa and Peter, 2009) have performed the laboratory, so-called tornado-like vortex flows are studied frequently, and numerical simulations in order to obtain the detailed information of that kind of strong swirling flow. Typically, Ward (Ward, 1972) firstly developed a laboratory simulator with a fan at the top to provide angular momentum, and succeeded in generation of many types of tornado-like vortex observed in nature. Wan and Chang (1972) measured radial, tangential and axial velocities with a three-dimensional velocity probe. They found that axial velocities near the vortex axis remain all positive and become strong for low swirl ratio, and are negative for high swirl ratio. Matsui and Tamura (2009) have conducted velocity measurement for tornado-like vortex generated by Ward-type simulator with Laser Doppler Velocimeter (LDV). However, in laboratory simulation, it was difficult to obtain detailed three-dimensional velocity and pressure field due to the strong turbulence motion. So far, numerical simulations have been conducted extensively to study the tornado-like vortex dynamics. In early stages, axisymmetric Navier–Stokes equation with constant viscosity in cylindrical coordinate to investigate the flow field of tornado-like vortex was used. Recently, Lewellen et al. (2007) used LES turbulence model to examine the sensitivity of vortex structure. Kuai et al. (2008) used the k-ε turbulent model to study parameter sensitivity for the flow field of a laboratory simulated tornado. They suggested that the numerical approach can be used to simulate the surface winds of a tornado and to control certain parameters of the laboratory simulator to influence the tornado-like vortex characteristics. However, the comparison between the numerical and laboratory simulated tornados is insufficient and mechanism of the formation of flow field has not been fully revealed. Furthermore, it is seems to that energy effect, which is maybe more important for the tornado-like vortex industrial application, is neglected in all these studies. The velocity field and energy characteristics of the tornado-like vortex have not been clarified enough. Related to flow and energy characteristics of tornado-like vortex are similar to those in the Ranque-Hilsch vortex tube (Ranque, 1933; Hilsch, 1947; Kurosaka, 2006; Eiamsa and Promvonge, 2008; Behera, Paul, Dinesh, and Jacob, 2008; Secchiaroli, Ricci, Montelpare, and Alessandro, 2009; Dutta, Sinhamahapatra, and Bandyopadhyay, 2013).

According to the Ranque-Hilsch principle, we designed a vortex jet flow device (that is, vortex jet tube) at Tsinghua University, Beijing, China, which was used to produce strong rotating jet with high vacuum and swirling in a limited space in order to study the tornado-like vortex. It's important to note that the vortex jet tube is a kind of application of Ranque-Hilsch effect and different to the vortex tube (VT) essentially, such as the high vacuum degree, double vortex, and long-narrow spiral jet and so on. This paper focuses on assessing numerical simulation of a tornado-like vortex jet flow based on Large-eddy simulation (LES) method, which is a more advanced Computational Dynamic Fluid (CFD) tool and extensively studied in recent years because it can give the detailed instantaneous flow structures and more exact statistical results than those given by the RANS. However, it is still a challenging task to simulate the tornado-like vortex (Jakirlic´, Hanjalic´, and Tropea, 2002; Yasutaka and Hirofumi, 2002). In particular, previous numerical studies have shown that the complex flow structure of tornado-like vortex depends on the initial axial, tangential and radial velocities of the flow. Variation of the axial, tangential and radial velocities results in various developments of the tornado-like vortices.

The objectives of the work reported herein were:

(a) To build a 3D mathematic model representing a tornado-like vortex jet flow explores parameter and model sensitivity. The effect of boundary conditions such as inlet, outlet, computational domain with respect to grid size and boundary conditions were studied.

(b) To use the numerical simulation to study the tornado-like vortex flow field and be compared with experimental data qualitatively, evaluating the capability of the model to simulate the velocity, temperature, and vacuum degree. The turbulent characteristics may play an important role in the flow and energy characteristic for this typical turbulent compressible flow.

(c) To use the velocity, vacuum degree and temperature from measurements to check how well the model reproduces the velocity, vacuum degree and temperature distribution. An understanding of these sensitivities will assist in the design of later numerical or laboratory experiments exploring the tornado-like vortex flow more closely.

(d) To understand the flow and the energy mechanism of tornado-like vortex jet, which will be used in combustion chamber of gas turbine in order to enhance combustion efficiency and probable energy effect in the future.

2. MATHEMATICAL MODELS

2.1 Governing Equations for LES

The filtered gas continuity, momentum, energy and gas state equations for compressible LES (Tim, Sanjiva, and Parviz, 1991; Erlebacher, Hussaini, Speziale, and Zang, 1992; Xu, Chen, and Lu, 2010)

of a tornado-like vortex jet flow can be obtained as, in which gravity effects are excluded.

$$\frac{\partial \rho}{\partial t}+\frac{\partial}{\partial x_i}\left(\rho \bar{u}_i\right)=0 \tag{1}$$

$$\frac{\partial}{\partial t}\left(\rho \bar{u}_i\right)+\frac{\partial}{\partial x_j}\left(\rho \bar{u}_i \bar{u}_j\right)= \frac{\partial}{\partial x_j}\left(\mu\left(\frac{\partial \bar{u}_i}{\partial x_j}+\frac{\partial \bar{u}_j}{\partial x_i}\right)-\frac{2}{3}\left(\mu \frac{\partial \bar{u}_j}{\partial x_j}\right)\delta_{ij}\right)-\frac{\partial \bar{p}}{\partial x_i}-\frac{\partial \tau_{ij}}{\partial x_j}+f_i \tag{2}$$

$$\frac{\partial\left(\rho \bar{h}\right)}{\partial t}+\frac{\partial}{\partial x_j}\left(\rho \bar{h} \bar{u}_j\right)=\frac{\partial}{\partial x_j}\left(\frac{\mu}{\Pr}\frac{\partial \bar{h}}{\partial x_j}\right)-\frac{\partial q_j^{sgs}}{\partial x_j}-\bar{q}_r \tag{3}$$

$$\bar{p}=\rho R \bar{T} \tag{4}$$

Where τ_{ij} is subgird-scale stress, $\tau_{ij} \equiv \rho\overline{u_i u_j}-\rho \bar{u}_i \bar{u}_j$. $\left(\bar{}\right)$means filtered mean value. The density fluctuations are neglected in Eqs (1) to (4), which is a reasonable approximation for the considered the flow when Mach-number is less than 5 (Tim, Sanjiva, and Parviz, 1991). f_i denotes body force, $f_i=\rho g$ and g is gravity acceleration.

2.2 Sub-Grid Scale Stress Model

Smagorinsky–Lilly model (standard Smagorinsky model (Smagorinsky, 1963), Germano model (dynamic Smagorinsky model) (Germano, Piomelli, Moin, and Cabot, 1991; You, Moin, 2007) and Subgrid-scale energy equation (SGS-k-equation, k^{sgs}) (Kim and Menon, 1995) stress model, used for closing the subgrid-scale turbulent viscosity, are adopted in this paper.

$$\tau_{ij}=-2\mu_t\left(\bar{S}_{ij}-\frac{1}{3}\bar{S}_{kk}\delta_{ij}\right)+\frac{2}{3}\rho k^{sgs}\delta_{ij} \tag{5}$$

$$\bar{S}_{ij}=\frac{1}{2}\left(\frac{\partial \bar{u}_i}{\partial x_j}+\frac{\partial \bar{u}_j}{\partial x_i}\right)$$

Where μ_t is subgrid-scale turbulent viscosity. $\bar{S}_{ij}$ denotes the rate-of-strain tensor for the resolved scale. In Smagorinsky–Lilly model,

$$\mu_t=\rho L_S^2\left|\bar{S}_{ij}\right|$$

$$L_S=min(\kappa\delta, C_s V^{1/3})$$

Where L_s is the mixing length for subgrid-scales, κ is the Von-Karman constant, 0.42, C_s is Smagorinsky constant ranged from 0.1 to 0.2 (Smagorinsky, 1963), δ is the distance to the closest wall and V is the volume of a computational cell. Germano model identity is used to calculate dynamic local values for C_s by applying the Smagorinsky model to both T_{ij} and τ_{ij}, which are different subgrid-scale stress term. The anisotropic part of τ_{ij}, in practice, requires stabilization. Often times this has been done by averaging Cs in a homogeneous direction. In cases where this is not possible, local averaging has been used in place of an average in a homogenous direction. The subgrid-scale kinetic energy is determined by equation (6) and formula (7) (Kim and Menon, 1995).

$$\frac{\partial \rho k^{sgs}}{\partial t}+\frac{\partial}{\partial x_i}\left(\rho \overline{u_j} k^{sgs}\right)= P^{sgs}-D^{sgs}+\frac{\partial}{\partial x_i}\left(\frac{\rho \nu_t}{\Pr_t}\frac{\partial k^{sgs}}{\partial x_i}\right) \tag{6}$$

$$k^{sgs}=\frac{1}{2}\left(\overline{u_i u_j}-\bar{u}_i \bar{u}_j\right) \tag{7}$$

Where k^{sgs} denotes the sub-grid scale kinetic energy, $\nu_t=C_\nu\left(k^{sgs}\right)^{1/2}\bar{\Delta}$ is the sub-grid scale eddy viscosity, and $\bar{\Delta}$ is the grid size. P^{sgs} is the shear production term closed by $P^{sgs}=\tau_{ij}\,\partial \bar{u}_i/\partial x_j$ and D^{sgs} is the dissipation term, $D^{sgs}=C_\varepsilon\left(k^{sgs}\right)^{3/2}/\bar{\Delta}$. C_ν and C_ε are empirical constants, which are taken as 0.067 and 0.916. $\Pr_t$ is turbulent Prandtl number 0.9 (Pitsch, 2006).

The sub-grid scale heat flux is closed using a gradient modeling as(Pitsch, 2006),

$$q_{j\,sgs}=\rho\left(\overline{u_j T}-\bar{u}_j \bar{T}\right)=\frac{\mu_t}{\sigma_T}\frac{\partial \bar{T}}{\partial x_j} \tag{8}$$

In Eqs. (8), the empirical constants σ_T =1.0.

The P1 model is used for the radiative heat transfer as (Pitsch, 2006),

$$-\bar{q}_r=aG-4a\sigma \bar{T}^4 \tag{9}$$

Where σ is the Stefan-Boltzmann constant 5.67× 10-8W/(m2•k4). a means the absorption coefficient a =0.1m^{-1} and G denotes the incident flux which is determined by solving the radiative transfer equation when a→0, →0.

3. THE GEOMETRIC MODEL AND COMPUTATIONAL DOMAIN

As shown in Fig.1, tornado-like vortex jet device used in this work is produced by our group at Tsinghua University, Beijing city, China, which is a novel design compared with traditional ones. The vortex jet tube has no moving parts and the fluid dynamic behavior is influenced by its geometry. Each part of the device has been investigated in order to have a correct understanding of the flow boundary conditions and to have some simplifications in the computational domain. In fact, the vortex jet tube used in this study has a radial inlet which in turn needs a particular component called ‘‘vortex generator (chamber)”, which is used to transform the radial air motion into a tangential one. The generator consisted of a swirl cavity and a long tube. Compressed air entered the cavity through the tangential slits to develop the swirling flow that then flows out through the tube into the room as a tornado-like vortex jet. A small pressure transducer in the bottom measured the initial pressure deficit, pvc0, in the cavity. Four nozzles (gas channel) are circumferentially arranged

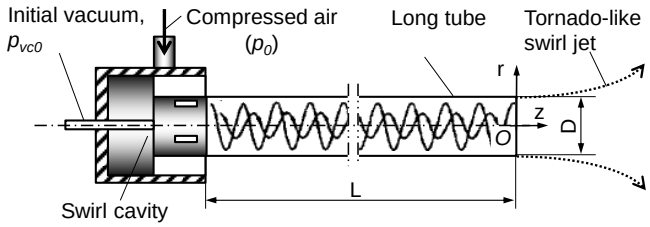

Fig. 1. Sketch of tornado-like vertex generator.

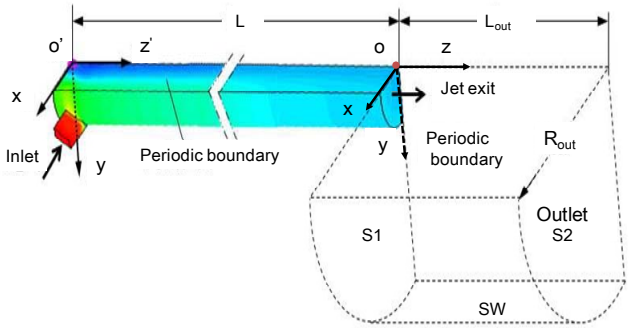

Fig. 2. Computational domain.

in the vortex chamber that allows the flow stream to arrive with high tangential velocity.

A complex computational domain as showed in Fig.2, including the surface of annular gap inlet and the virtual surface that has been used as computational virtual surface named as S1, SW and S2. These surfaces should be suitable for computational simulation without influence to the calculation of internal core zone according to the specificity of the vortex jet flow in this kind of devices. Meantime, two sets of coordinate system, x-y-z and x-y-z' had been set up for computational domain as shown in Fig.2. The dimensionless coordinate parameters are z/D and r/R, which follows the coordinate system transformation rule of z'= z-0.2 with the same x, y coordinate and D=0.01m, R=0.005m.

4. NUMERICAL PROCEDURE AND BOUNDARY CONDITIONS

In the present work, the LES was made for a tornado-like vortex jet flow measured by Huang et al. at Tsinghua University, China. The whole computational domain surrounded by the dashed line and tornado-like vortex jet tube, as shown in Fig.2. The detail flow conditions at the computational model are shown in table 1. Four boundaries of the domain include the inlet, the outlet, the periodic boundary, and wall boundary. At the inlet, Dirichlet boundary conditions (first-type boundary conditions) are used, which is pressure inlet condition. Pressure outlet boundary conditions are used at the outlet. All of those boundary conditions are much easier than the treatment of a solid wall, in which the boundary layer needs to be considered. Compressed air is obtained by 300K through the inflow channel. In the current simulations turbulence is specified at the inlet with a turbulence intensity 10% and turbulence viscosity ratio 10. Simulations with different turbulence at the inlet like 1% and 1 were performed and it was observed that they did not produce any significant change in the results. At the tube wall, no-slip wall boundary condition with the Enhanced Wall Function model is used. In this near-wall modeling technique the viscous sub-layer is also resolved where y+ is the distance to the wall at the wall-adjacent cell (Secchiaroli, Ricci, Montelpare, and Alessandro, 2009). In the current simulations, y+=1.8. When a wall-adjacent cell is in the laminar sublayer, the wall shear stress is obtained from the laminar stress–strain relationship. If the mesh cannot resolve the laminar sublayer, it is assumed that the centroid of the wall-adjacent cells fall within the logarithmic region of the boundary layer, and the law-of-the-wall is adopted (Secchiaroli, Ricci, Montelpare, and Alessandro, 2009). In the tornado-like vortex jet flow, a flow with both axial and radial pressure gradients appears, but the radial pressure gradient is dominant comparing with the axial pressure gradient in the near wall region, which implies that the wall function can be used here because the wall-adjacent cells are in the laminar sublayer in most of the region. As shown in Fig.2, computation domain has a diameter of Rout=0.4m and a length of Lout=2.0m. The grid number is from 2,800,000 to 4,300,000. Different computational grids were designed for numerical simulation. LES simulations were performed over periodic grid in 1/4 zone, where a complete three-dimensional grid was used with structured Cartesian cells and near wall refinement. Grid in the computational domain is generated by ICEM CFD 14.5 and is divided into 22 sub-volumes to get a better control of cells skewness and dimension.

Table 1 Flow conditions at the computational model

parameters	value
Inlet pressure p0 (gauge pressure, kPa)	100-400
Inlet temperature T0 (K)	300
Inlet surface A (m^2)	5.0E-06
Vortex jet tube diameter D (m)	0.01
Axial extension tube L (m)	0.19
Angle of inclination (Inlet channel with axis, °)	18

Table 2 LES computational conditions of different case

Case number	Number of cells	Turbulent model
Case 1	4,300,000	Dynamic Smagorinsky
Case 2	3,800,000	--
Case 3	2,800,000	--
Case 4	4,300,000	--
Case 5	4,300,000	--
Case 6	4,300,000	--

S1 position/ boundary	SW position/ boundary	S2 position/ boundary
Move 0.03m(z'=0.17m)/ pressure inlet	Rout=0.3m/ pressure inlet	Lout=2.0m/ pressure outlet
Move 0.03m (z'=0.17m)/ pressure inlet	Rout=0.3m/ pressure inlet	--
Move 0.03m (z'=0.17m)/ pressure inlet	Rout=0.3m/ pressure inlet	--
Move 0.03m (z'=0.17m)/ pressure inlet	Rout=0.4m/ pressure outlet	--
Move 0.03m(z'=0.17m)/ pressure inlet	Rout=0.4m/ pressure inlet	--
Move 0.12m(z'=0.08m)/ pressure inlet	Rout=0.4m/ pressure inlet	--

The time step is taken as 1e-6s. On numerical scheme, second order upwind and third order MUSCL (monotonic upstream-centered scheme for conservation laws) are adopted for the advection terms while second order central differencing scheme is applied for the diffusion terms. SIMPLE algorithm is used coupling between the velocity and pressure. Random fluctuations are superposed to the inlet plane which means that turbulence intensity is imposed at the inflow. For grid nodes near the wall, the wall function approximation is used to bridge the wall. The convergence criteria are mass, momentum sources less than 10−4 and energy source less than 10−6, respectively. Ansys Fluent14.5 was used in this paper. The computational time needed to produce reliable results is at least 24 hours on the HPC (High Performance Computing) of Intel(R) 700 Core(TM) and 2.4 GHz per processor. Numerical simulations were performed on that workstation and computational time is almost independent of turbulent closure models. Table 2 shows computational conditions of different case assessing numerical simulation on LES.

The boundary conditions are as follows:

(i) Stagnation boundary condition at the inlet is specified with static gauge pressure of 100-400kPa and static temperature of 300K.

(ii) Pressure boundary condition at outlet with static absolute pressure of 101kPa and static temperature of 300K.

(iii) No slip and Zero gradient of temperature at the wall.

5. RESULTS AND DISCUSSION

5.1 Grid Density Sensitivity Analysis

In order to investigate the sensitivity of the numerical simulation results, the grid size solution of computations was completed. A grid independence procedure was implemented with different numbers of cells allowing a better period of the cells in axial and radial direction. A grid refinement sketch is presented in Fig.3. Axial refinements were performed at the inlet section, near the tube exit and tornado-like vortex core region. In this way, three-dimensional model were composed of about 4,300,000 elements. Coarser grids were developed to perform grid independence analysis about 2,800,000 and 3,800,000 elements. Figs.4-a, 4-b and 4-c present a comparison of the simulated radial profiles of the vacuum, temperature and axial velocity at two different section distanced from the rotating jet exit in the axial direction using those different grids, where x-y-z coordinate system is used, and D=0.01m. All grids capture well the characteristics of the velocity and pressure reasonably. The fine mesh provides a more

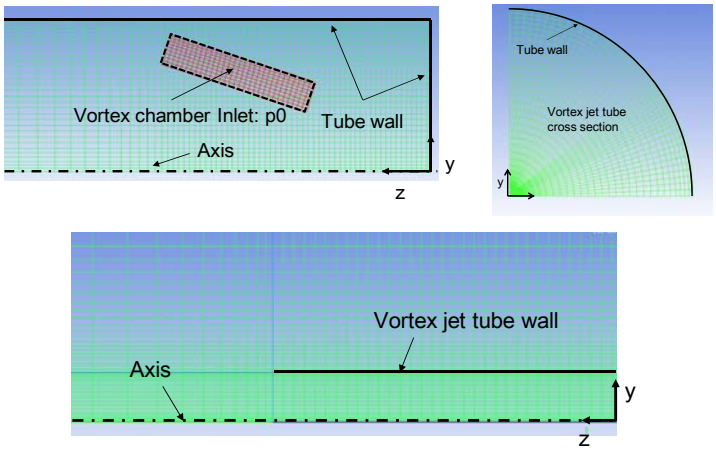

Fig. 3. Computational grid refinement used in LES.

reasonable resolution. It was correctly anticipated to improve the results in the vicinity of the outlet of rotating jet tube. The pressure in the vicinity of the exit of rotating jet tube is captured more reasonably. As is shown the differences between the results obtained with the coarse and fine meshes are qualitatively similar and the differences are sufficiently small to justify the use of the coarse mesh for sensitivity analysis. The computational cost of the fine mesh resulted in an increase of over 80% compared with coarse mesh with a reasonable accuracy. A mesh sensitivity study of using the present mathematical model also shows that the predicted global properties, i.e. pressures, match well between a coarse mesh and a fine mesh. A finer mesh that reduced the average grid size was also tested in this study. The results indicated no noticeable change in predicted mean pressure, velocity and temperature. The current fine mesh is adequate for the present tornado-like vortex jet flow application.

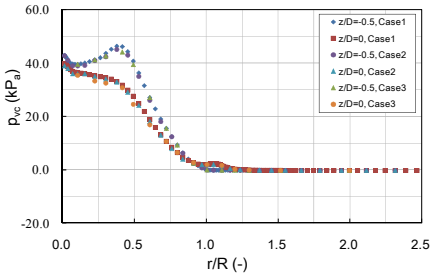

Fig. 4-a. Radial profiles of the vacuum degree at different z/D with different grid density.

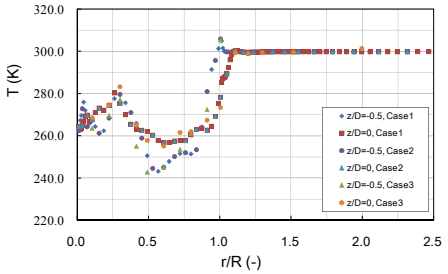

Fig. 4-b. Radial profiles of the temperature at different z/D with different grid density.

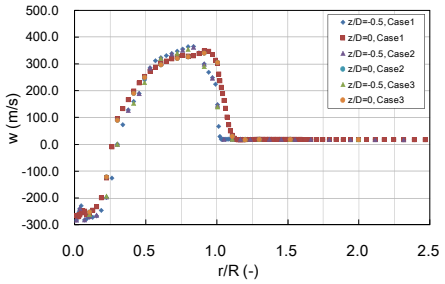

Fig. 4-c. Radial profiles of the axial velocity at different z/D with different grid density.

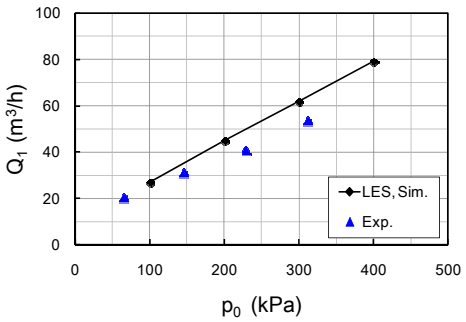

Fig. 5. Comparison between LES and experiment for standard volume flow rate relate with p0

5.2 Feasibility validation of LES and the flow characteristics

5.2.1 Feasibility Validation of LES

Fig.5 shows statistically averaged standard gas volume flow rate with different inlet pressure p0, and its comparison with the measurement results. Computational conditions are given in table 2 case 5. It can be seen that numerical results is slightly higher than the measured values at lower inlet pressure p0, and has an error margin of 15% at higher inlet pressure p0. It is because of the simulation conditions are ideal gas. The real fluid resistance loss is relatively larger. So the computed results obviously higher with large p0, which resulting in an unrealistic condition for jet impingement applications. Fig.6 gives the vacuum

Table 3 Maximum temperature difference of internal flow and vacuum degree on tube bottom

Inlet pressure, p0 (kPa)	Maximum temperature difference, ΔT (K)	Maximum vacuum degree (LES), p_{vc} (kPa)	Maximum vacuum degree (Exp.), p_{vc} (kPa)
100	41.88	15.5	--
200	71.52	31.5	--
300	87.21	39.7	53.0
400	97.85	44.4	--

degree distribution along the axis in axial direction with inlet pressure p0=300kPa, which demonstrates a good agreement with experimental data quantitatively and seems more representative of the tornado-like vortex jet flow pressure profiles.

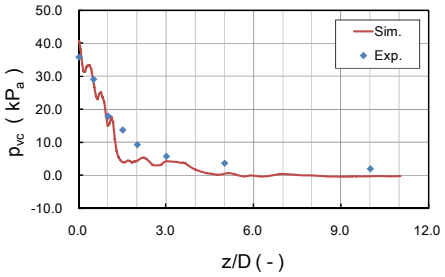

Fig. 6. Axial vacuum degree profile between simulated and measured (Parameter: p0=300 kPa).

Table 3 gives the several parameters of simulated results and experimental ones on maximum temperature difference of internal flow and vacuum degree on tube bottom (o' point shown in Fig.2). Obviously, maximum temperature difference and maximum vacuum increased with the increase of p0. When p0 = 300 kPa, maximum temperature difference arrived at 87 K and maximum vacuum degree was 40kPa. The tornado-like vortex jet flow demonstrate visible the energy separation and vacuum effect. Furthermore, the maximum temperature difference and vacuum degree increased slowly with p0, because the gas inlet velocity has been gradually close to the speed of sound. Hence, an accurate numerical analysis would be the effective way to obtain information about velocity, pressure and temperature fields in the simulation domain. However, there is still a great difference between numerical results and experimental ones and has an error margin of 20% under p0=300kPa.

5.2.2 Flow Characterizes

Figs.7 and 8 show the predicted instantaneous vorticity map at the section of y=0.0m and three dimensional iso-vorticity structures at p0=300kPa respectively. In axial direction, vorticity is appearing near the whole axis zone. Obviously, it is because of radial pressure gradient. It can be seen that the vortices near the tube exit, shear region of swirling jet flow, are intensified to become large vortices and finally are weakened in the downstream region and radial direction. With the increase of radial distance, vortices gradually disappeared where axial velocity and swirl intensity decrease with the decrease of vacuum degree quickly. In addition, tornado-like vortex jet flow does not like the common industrial swirl flow, which has turbulent jet inertial effect. That mainly is because of the center of the vacuum region and the surrounding atmosphere formed the high radial pressure gradient. The fluid was accelerated due to the centripetal force and force produced by the rotating jet.

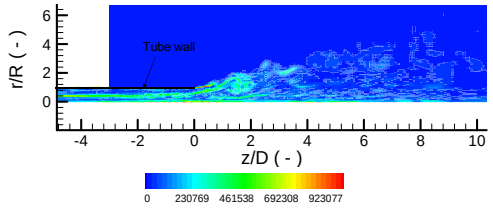

Fig. 7. Vorticity map at the section of y=0.0m, ω (s-1) (Parameter: p0=300 kPa).

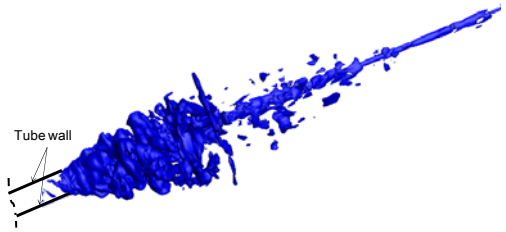

Fig. 8. Three dimensional iso-vorticity structure of ω=40000 s-1(Parameter: p0=300 kPa).

According to the vortex jet flow feature, where the ratio of the axial velocity and tangential velocity are important along the axial direction. Hence, we get the streamline (spiral line) at different vortex jet section as shown in Fig.9, where green spiral line at the center of the tube demonstrate gas flows moves slower with negative axial velocity and faster near the wall with positive axial velocity because of strong swirling jet. Radial velocity is smaller than axial velocity. There has strong swirling intensity in the core of vortex and external low speed flow surrounding the vortex has little influence on the body structures of vortex. Two kind of spiral line are shown in (a), (b) and (c) of Fig.9, and spiral angle increases along the axial direction. The flow field presents a specific characterize of double-vortex where both internal vortex and outer vortex do co-exist.

Fig.10 gives the pressure distribution (left) and partial enlarged (right) in inertial tube at section y=0.0m. It can be seen that pressure distribution, similar to conventional Vortex Tube flows, the

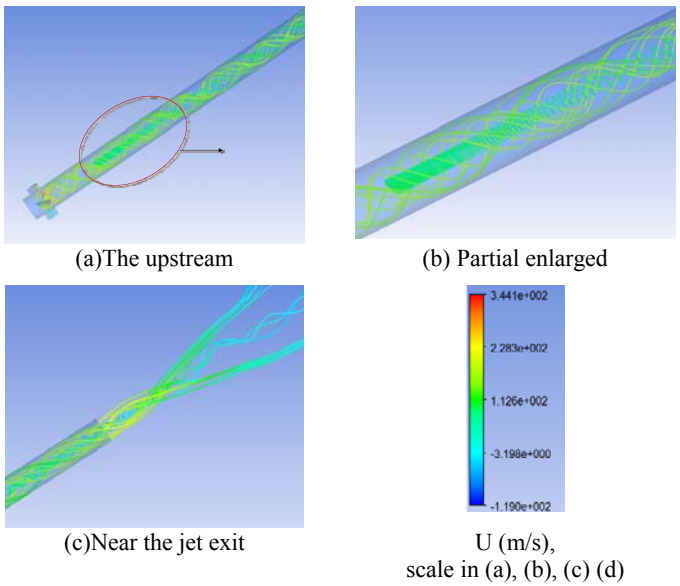

(a)The upstream (b) Partial enlarged

(c)Near the jet exit U (m/s), scale in (a), (b), (c) (d)

Fig. 9. Streamline (spiral line) at different vortex jet tube position (Parameter: p0=300 kPa).

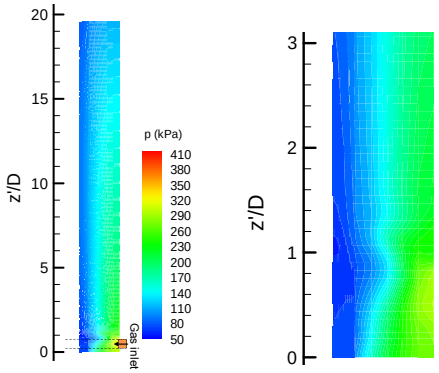

P (kPa)

Fig. 10. Pressure (left) and partial enlarged (right) distribution (Parameter: p0=300 kPa, y=0.0 m).

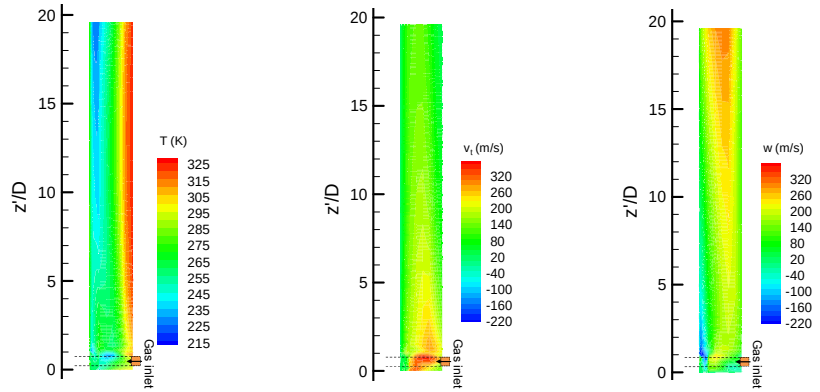

Fig. 11. Temperature, tangential velocity and axial velocity distribution (Parameter: p0=300 kPa, z/D=0.5, y=0.0 m).

tangential flow through the inlet channel is forming
strong swirl flow along the radial direction and low pressure vacuum along the axis. There is a great pressure gradient in the radial direction. As shown in the tangential velocity and axial velocity distribution of the Fig.11 (middle and right), wall friction makes the tangential velocity slowing. Tangential and axial flow is gradually into the fully developed. Meantime, the axial velocity presents the increasing characteristics as the tangential velocity. From the temperature distribution of Fig.11 (left), energy separation

effect is very obvious, and along the axial direction also has a process of constant development. The highest temperature near the wall was about 52 ℃. The above results suggest that the formation of tornado-like vortex is the results of the firstly condition of inlet pressure p0, i.e. is the results of strong swirling. A sketch of instantaneous streamlines with the axial velocity near the vortex jet exit (p0=300kPa, z/D=0.5) obtained by LES are showed in Fig.12. It can be seen that strong swirling feature of tornado-like vortex is presented. In internal vortex, the axial velocity is positive and is negative in outer vortex.

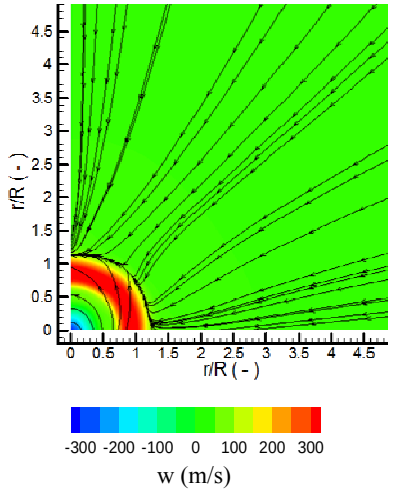

Fig. 12. Axial velocity and streamline in a cross section of the jet (Parameter: p0=300 kPa, z/D=0.5).

Through the above analysis, the tornado-like vortex jet flow characterizes are presented generally, which suggest that LES can be used in simulating a tornado-like vortex jet flow. However, it is still a big challenge in predicting accurately the specific swirling jet flow in details. Fig.13 gives radial distribution of measured vacuum degree and temperature with p0=300kPa. The experimental conditions are consistent with the computational model in addition to the inlet channel which has an angle of inclination with 0° between gas inlet channel and axis. To be sure, it still has important comparability of tornado-like vortex flow characteristic qualitatively. A "volcanic vent" distribution for radial vacuum profile is shown in Fig.13 (left) and single peak feature of radial temperature distribution is shown in Fig.13 (right) obviously. Moreover, the peak of "volcanic vent" is located at r/R=0.8. The vacuum degree decreases and the temperature increases along the axial direction.

6. CONCLUSION

Assessment of the 3D mathematical model in conjunction with the compressible flow to resolve strong tornado-like vortex jet turbulent flow and energy effect has been performed. Commercial CFD codes Ansys Fluent 14.5 was used to perform numerical simulations by LES. Numerical results suggest that CFD simulation of the tornado-like vortex jet flow and temperature field is still a challenging task because of its compressibility, turbulence, high vacuum and strong swirling. Moreover, experimental measurements velocity and temperature fields of the internal and outer space domain are still necessary for the verification, which are very difficult to obtain accurately. Flow patterns in different sections show a quite different with the results available by this works. Strong differences between numerical results and experimental ones are showed on axial velocity profiles, vacuum degree profiles and temperature distribution in radial direction. LES results show a "volcanic vent" trend for radial vacuum profile. All the simulations confirmed that radial velocity is very small when compared with axial and tangential ones. Hence, this component could be ignored in the analysis of the energy separation process as in a recent numerical study. In the prediction of the temperature field shows a lower temperature near the tube axis and a considerably different static temperature radial distribution. Temperature radial profiles demonstrate a qualitative different with experimental data.

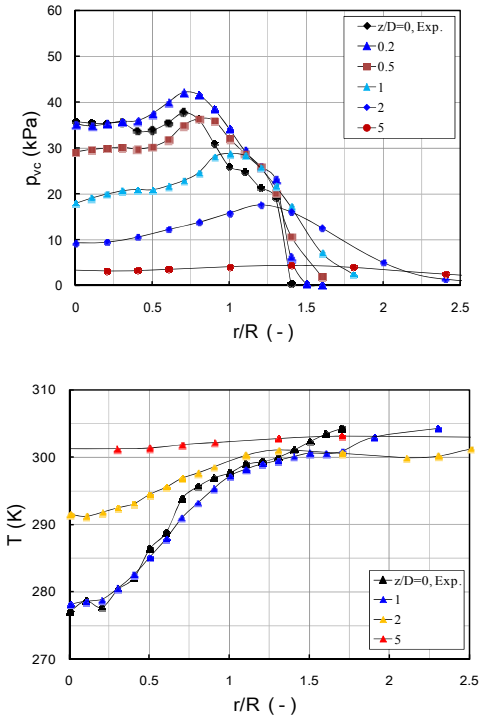

Fig. 13. Radial distribution of measured vacuum degree and temperature with p0=300kPa.

A qualitative estimation of LES for tornado-like vortex jet flow was performed by tuning the grid finely, different computation domain, and SGS turbulent model that were used in the prediction of temperature, velocity and vacuum degree components. The results obtained by CFD can be used when modelling inertial and outer space domain of rotating jet flow in the numerical simulations. It is important information needed for

the estimation of tornado-like vortex jet flow capability. However, the present LES numerical results are not still consistent with the experimental ones. That is to say, LES still cannot predict this kind of tornado-like vortex jet flow accurately. One of reasons is that grid number in the core region of tornado-like vortex is not enough, especially in the region with extreme gradient of the velocity and temperature. Another, maybe the most import reason and should be studied and developed in the future, is that SGS model is not suitable for the special vortex jet flow.

ACKNOWLEDGEMENTS

The financial supports sponsored by the Project of National Natural Science Foundation of China under the Grant No. 51776221, 51266008, No. 51176092 and International Clean Energy Talent Program (iCET) of China Scholarship Council.

REFERENCES

Behera, U., P. J. Paul, K. Dinesh and S. Jacob (2008). Numerical Investigation on flow behavior and energy separation in Ranque–Hilsch vortex tube. Int J Heat Mass Tran. 51, 6077-6089.

Diwakar, N. and H. Horia (2012). Large eddy simulations of translation and surface roughness effects on tornado-like vortices. J Wind Eng Ind Aerod. 104, 577-584.

Dutta, T. and K. P. Sinhamahapatra, S. S. Bandyopadhyay (2013). CFD Analysis of Energy Separation in Ranque-Hilsch Vortex Tube at Cryogenic Temperature. J Fluids. l44, 1-14.

Eiamsa-ard, S. and P. Promvonge (2008). Review of Ranque–Hilsch effect in vortex tubes. Renew Sust Energ Rev. 12, 1822–1842.

Erlebacher, G., M. Y. Hussaini, C. G. Speziale and T. A. Zang (1992). Toward the large-eddy simulation of compressible turbulent flows. J Fluid Mech. 238, 155-185.

Germano, M., U. Piomelli, P. Moin and W. H. Cabot (1991). A dynamic subgrid-scale eddy viscosity model. Phys Fluids. A (3), 1760-1765.

Hilsch, R. (1947). The use of the expansion of gases in a centrifugal field as cooling process. Rev Sci Instrum. 18, 108–113.

Ishihara, T., S. Oh and Y. Tokuyama (2011). Numerical study on flow fields of tornado-like vortices using the LES turbulence model. J Wind Eng Ind Aerod. 99, 239-248.

Jakirlic, S., K. Hanjalic and C. Tropea (2002). Modeling rotating and swirling turbulent flows: A Perpetual Challenge. *AIAA J. 40*(10), 1984-1996.

Jones, R. D. (2015). A review of supercell and tornado dynamics. Atmos Res.158-159, 274-291.

Kim, W. and S. Menon (1995). A new dynamic one-equation subgrid-scale model for large eddy simulation. In 33rd Aerospace Sciences Meeting and Exhibit, Reno, NV.

Kuai, L., F. L. Haan, W. A. Gallus and P. P. Sarkar (2008). CFD simulations of the flow field of a laboratory simulated tornado for parameter sensitivity studies and comparison with field measurements. Wind Struct. 11(2), 1–22

Kurosaka, M. (2006). Acoustic streaming in swirling flows and the Ranque–Hilsch (vortex tube) effect. J Fluid Mech.124(124), 139–172.

Lewellen, D. C. and W. S. Lewellen (2007). Near-surface intensification of tornado vortices. J Atmos Sci. 64, 2176–2194.

Lisa, S. and N. Peter (2009). On the theory of intensity distributions of tornadoes and other low pressure systems. Atmos Res. 93, 11-20.

Matsui, M. and Y. Tamura (2009). Influence of swirl ratio and incident flow conditions on generation of tornado-like vortex. Proceedings of EACWE5.

Pitsch, H. (2006). Large-Eddy Simulation of Turbulent Combustion. Annu Rev Fluid Mech. 38, 453– 482.

Ranque, G. J. (1933). Experiments on expansion in a vortex with simultaneous exhaust of hot air and cold air. Le Journal dePhysique et le Radium. 4, 112–114.

Richard, R. (2013), The fluid dynamics of tornadoes. Annu Rev Fluid Mech. 45, 59-84.

Secchiaroli, A., R. Ricci, S. Montelpare and V. D. Alessandro (2009). Numerical simulation of turbulent flow in a Ranque–Hilsch vortex tube. Int J Heat Mass Tran. 52, 5496-5511.

Smagorinsky, J. (1963). General circulation experiments with the primitive equations. Ⅰ: the basic experiment. Mon Weather Rev. 91, 99-164.

Tari, P. H., R. Gurka and H. Hangan (2010). Experimental investigation of tornado-like vortex dynamics with swirl ratio: The mean and turbulent flow fields. J Wind Eng Ind Aerod. 98, 936-944.

Tim, C., K. L. Sanjiva and M. Parviz (1991). The free compressible viscous vortex. J Fluid Mech. 230, 45-73.

Wan, C. A. and C. C. Chang (1972). Measurement of the velocity field in a simulated tornado-like vortex using a three-dimensional velocity probe. J Atmos Sci. 29, 16–127.

Ward, N. B. (1972). The exploration of certain features of tornado dynamics using a laboratory model. J Atmos Sci. 29, 1194–1204.

Xu, C. Y., L. W. Chen and X. Y. Lu (2010). Large-eddy simulation of the compressible flow past a wavy cylinder. J Fluid Mech. 665, 238-273.

Yasutaka, N. and H. Hirofumi(2002). An improved turbulence model for rotating shear flows. J Turbul. 3(6), 1-14.

You, D. and P. Moin (2007). A dynamic global-coefficient subgrid-scale eddy-viscosity model for large-eddy simulation in complex geometries. Phys Fluid. , 19(6), 229-244.